Converting a broad matrix metalloproteinase family inhibitor into a specific inhibitor of MMP-9 and MMP-14

Jason Shirian[1], Valeria Arkadash[2], Itay Cohen[2], Tamila Sapir[1], Evette S. Radisky[3], Niv Papo[2*], and Julia M. Shifman[1*]

[1]Department of Biological Chemistry, The Alexander Silberman Institute of Life Sciences, The Hebrew University of Jerusalem, Jerusalem, Israel

[2]Department of Biotechnology Engineering and the National Institute of Biotechnology in the Negev, Ben-Gurion University of the Negev, Beer-Sheva, Israel

[3]Department of Cancer Biology, Mayo Clinic Comprehensive Cancer Center, Jacksonville, Florida, USA

[*]**To whom correspondence should be addressed. E-mail: jshifman@mail.huji.ac.il; papo@bgu.ac.il.**

Abstract

MMP-14 and MMP-9 are two well established cancer targets for which no specific clinically relevant inhibitor is available. Using a powerful combination of computational design and yeast surface display technology, we engineered such an inhibitor starting from a non-specific MMP inhibitor, N-TIMP2. The engineered purified N-TIMP2 variants showed enhanced specificity towards MMP-14 and MMP-9 relative to a panel of off-target MMPs. MMP-specific N-TIMP2 sequence signatures were obtained that could be understood from the structural perspective of MMP/N-TIMP2 interactions. Our MMP-9 inhibitor exhibited 1000-fold preference for MMP-9 vs. MMP-14, which is likely to translate into significant differences under physiological conditions. Our results provide new insights regarding evolution of promiscuous proteins and optimization strategies for design of inhibitors with single-target specificities.

Introduction

Matrix metalloproteinases (MMPs) belong to a family of over twenty MMPs and twelve homologous ADAMs proteases, enzymes that are respectively responsible for degradation of the extracellular matrix and membrane proteins [1]. MMPs differ in domain composition and size, yet all of them share a similar catalytic domain with a Zn^{2+} ion in the active site. MMPs are first produced in an inactive form and are activated by the cleavage of a pro-domain by certain MMPs or other proteases. MMP function is important in biological processes involving tissue remodeling, such as development and immune response [2].

Upregulation of MMPs or lack of MMP inhibition leads to various diseases including arthritis, chronic obstructive pulmonary disease, inflammatory bowel diseases, sepsis and various types of cancer [2]. In cancer, some MMPs play a crucial role in angiogenesis, metastasis and other aspects of tumor growth through cleavage and activation of a variety of different proteins [3-5]. The unhindered digestion of the extracellular matrix by specific MMPs such as MMP-2 and MMP-9 allows for tumor progression and cancer cells to invade and traverse from one tissue to another, resulting in the appearance of new tumors, and the activity of other MMPs, such as membrane bound MMP-14 (also called MT1-MMP) that promote cancer by activating other MMP family members [6]. Inhibition of particular MMPs could hence reverse cancer progression and reduce the spread of cancer cells.

Due to their importance to disease, MMPs have been the target for drug design efforts over the past thirty years, and several small molecules were developed early on for MMP inhibition [3]. Yet, all of them have failed in clinical trials [7]. The major reason for the failure of these drugs was their low specificity: small-molecule MMP inhibitors were designed to bind to the active-site Zn^{2+} and hence reacted with Zn^{2+} and other heavy metals in various proteins in the body and thus were highly toxic. In addition, drugs directed at multiple MMP family members elicited unexpected effects due to diverse MMP activities. In fact, some MMPs have been documented to play essential roles and even anti-tumorigenic roles [8-10], pointing to the importance of developing selective inhibitors that target only one or a narrow range of MMPs.

Such high specificity, while difficult to obtain with small molecules, could be achieved in protein-based inhibitors [11-14]. Proteins possess a greater potential for high specificity due to their large interaction surface that involves not only the highly conserved catalytic site but also more variable surrounding residues. In this respect, antibodies have been developed that specifically target MMP-9 [15] and MMP-14 [16, 17], proving the possibility of engineering a type-specific MMP inhibitor. Besides antibodies, other attractive scaffolds for MMP inhibitor design are the natural broad inhibitors of the MMP family, tissue inhibitors of metalloproteinases (TIMPs). The mammalian TIMPs include four

homologous proteins (TIMP1–4) that exhibit slightly different preferences for various MMPs [18]. The advantage of using TIMPs for MMP inhibitor design is their already high affinity towards various MMPs (10^{-10}-10^{-9} M), no toxicity, no immunogenicity and their smaller size that facilitates their easy production by microbial expression and supplies them with better tissue perfusion rates in comparison to antibodies. To this end, TIMPs have been already a subject of several protein engineering studies [19-22].

For this study, as a scaffold for MMP inhibitor design, we chose the N-terminal domain of TIMP-2 (N-TIMP2), consisting of 126 amino acids. The isolated N-TIMP2 remains a strong inhibitor of various MMPs [23, 24] and is more easily expressed in bacterial cultures compared to the full-length TIMP2. Most importantly, N-TIMP2 has a smaller protein interaction network compared to the full length protein; it cannot participate in interactions with the MMP hemopexin-like domain, thus losing its ability to activate certain MMPs [25]. The crystal structures of TIMP2-MMP complexes [19, 26-29] show that binding of N-TIMP2 to MMPs is mediated by four discontinuous regions (Figure 1A). These regions include the N-TIMP2 N-terminal region that comes in close proximity to the highly-conserved enzyme active site and three loops (35-42, 66-72, and 97-99). While previous TIMP protein engineering studies mostly focused on mutating the N-terminal residues, we decided to focus on the loops that interact with less conserved residues further away from the enzyme active site. Such a strategy is likely to yield inhibitors that can discriminate between different MMPs.

The goal of this work was to evolve the multispecific inhibitor N-TIMP2 into a high-affinity and high-specificity inhibitor of one out of two different MMP family members: a membrane-bound MMP, MMP-14, or the secreted gelatinase, MMP-9. The catalytic domains of MMP-14 and MMP-9 (termed MMP-14_{CAT} and MMP-9_{CAT}, respectively) are structurally very similar (RMSD of 0.6 Å) showing an overall sequence identity of 45% and 66% identity among the residues that contact N-TIMP2 (Figure 1A and B). N-TIMP2 is a prototypical multispecific protein [30], whose sequence is a compromise for interactions with all MMP family members and thus is not optimal for interactions with each specific MMP [31, 32]. Recent studies on other multispecific proteins demonstrated that such proteins could be converted into highly specific binders of a particular target either through computational methods [33-35] or directed evolution approaches [36, 37].

In our previous work [38], we used the computational saturation mutagenesis protocol [35, 39] to explore the effect of all single mutations in the N-TIMP2 binding interface on N-TIMP2's binding affinity and specificity to MMP-$14_{CAT.}$ Our computational results pointed to a high frequency of mutations that enhance N-TIMP2's affinity and specificity toward MMP-14. Experimental results confirmed our predictions, identifying ten affinity-enhancing mutations and eleven specificity-enhancing mutations for MMP-14 relative to MMP-9. However, the enhancement in binding specificity remained relatively low for single mutations, not exceeding a factor of ten. Clearly, introduction of multiple mutations into N-

TIMP2 would be required to achieve further improvements. In the present study, we thus constructed a small combinatorial library of N-TIMP2 mutants that is rich in affinity- and specificity-enhancing mutations and used yeast surface display (YSD) technology [40] to select N-TIMP2 variants that bind selectively to MMP-14_{CAT} and separately to MMP-9_{CAT}. Our results show that selective N-TIMP2 inhibitors could be found and the acquired mutations contained specific signatures that define specificity for each of the MMPs.

Materials and Methods

Preparation of N-TIMP2 Libraries for YSD

The pCHA yeast surface display plasmid [41] was used for displaying N-TIMP2 WT and mutants on the yeast surface with a free N-terminus. The library of N-TIMP2 mutants was constructed using an assembly PCR method (see Supporting Information) randomizing positions 4, 6, 35, 38, 68, 71, 97, 99 to particular amino acids specified in Table 1. The transformation of the library to yeast was performed by simultaneously transforming the amplified mutant N-TIMP2 fragments with a pCHA[VK1] vector linearized by BamHI-HF and Nhe-HF restriction enzymes (New England Biolabs) into a competent EBY100 *Saccharomyces cerevisiae* yeast strain by electroporation.

FACS Analysis and Sorting

Growth of yeast (EBY100) cells, FACS analyses and sorting of libraries was performed as in Arkadash et al. [42]. For the detection of binding to MMP-14_{CAT}, the cells were incubated with MMP-14_{CAT} labelled with DyLight-488 for 1 hour on ice. An identical process was performed for detection of MMP-9_{CAT} binding, where MMP-9_{CAT} is labelled with DyLight-650. Three rounds of selection were performed with lowering the concentration of the target MMP and raising the concentration of the off-target MMP (see Figure S2).

Yeast Library Sequencing

After each round of sorting, cells collected from the flow cytometry sorter were grown in SDCAA medium (0.54% Na_2HPO_4, 0.86% $Na_2HPO_4{\cdot}H_2O$, 1.5% agar, 2% dextrose, 0.67% yeast nitrogen base, 0.5% Bacto casamino acids) supplemented with chloramphenicol (25 µg/ml) for ~36 hrs. 10 µl of resulting culture was diluted in SDCAA to a volume final of 2 ml, 20 µl of this diluted solution was plated on SDCAA agar plates supplemented with chloramphenicol (25 µg/ml). Single colonies were picked and served as input for colony PCR and subsequent sequencing (see Supporting Information for details).

N-TIMP2 Expression and Purification

The N-TIMP2 mutant genes were transferred from the pCHA plasmid obtained from yeast lysates (lysed by boiling in 0.02 M NaOH) to the pPICZαA *P. pastoris* expression vector by transfer PCR [43].

PCR products were subsequently linearized with SacI (New England Biolabs) transformed into chemical competent DH5α *E. coli*. The transformed bacteria were plated on LB agar plates containing 25 μg/ml Zeocin (InvivoGen, CA, USA). After an overnight incubation at 37°C, three colonies were chosen for growth in liquid LB medium at 37°C for ~16 hours, the plasmid was purified, and the correct sequence was verified by sequencing. Bacterial cultures possessing plasmids encoding for the correct sequence were grown for ~16 hours at 37°C for large scale plasmid purification by maxiprep (Geneaid, Taiwan). The purified plasmid was then transformed to X33 *P. pastoris* yeast and recombinant protein production was induced as described in our previous work [42].

The proteins were purified as described in our previous work [42]. Protein concentrations were determined by UV-Vis absorbance at 280 nm, with an extinction coefficient (ε_{280}) of 13,325 $M^{-1}cm^{-1}$ for WT N-TIMP2 and all its mutants.

MMP Enzyme Expression and Purification

The human MMP-9 catalytic domain (MMP-9_{CAT}), residues 107–215, 391–443, was expressed and purified as previously described [15], with the following modifications; the gene was expressed in Bl21(DE3)pLysS *E.coli* cells in a pET28 vector (with an N-terminal 6×His tag) and induced with 1mM isopropyl β-D-1-thiogalactopyranoside (IPTG) overnight at 30°C. The enzyme was nickel affinity purified, subsequently purified by anion exchange chromatography and then by size exclusion chromatography. The catalytic domains of MMP-1, MMP-2, MMP-10, and MMP-14 (MMP-1_{CAT}, MMP-2_{CAT}, MMP-10_{CAT} and MMP-14_{CAT}, respectively) were expressed and purified as previously described [29, 42, 44].

Enzymatic Activity Assay of N-TIMP2:MMP binding

Varying concentrations of N-TIMP2 were incubated with 0.5 nM MMP-1_{CAT}, 6 nM MMP-2_{CAT}, 0.1 nM MMP-9_{CAT}, 0.5 nM MMP-10_{CAT}, 0.2 nM MMP-14_{CAT} under conditions similar to that described in [42]. Fluorescence resulting from cleavage of fluorogenic substrate was measured at 395 nm, at least every ten seconds for at least 6 minutes, immediately after addition of fluorogenic substrate with irradiation at 325 nm on a Biotek Synergy H1 plate reader (BioTek, VT, USA). At least three assays were performed for each N-TIMP2 protein.

K_i^{app} Determination

Initial velocities of the enzymatic (MMP) cleavage of the fluorogenic substrate were derived from the fluorescence generated by this cleavage. Fraction of MMP activity was determined from the enzymatic assay, expressed as the inhibited velocity (V_i) divided by the uninhibited velocity (V_0), and was plotted

against the corresponding concentration of N-TIMP2. From this plot the apparent K_i (K_i^{app}) value was solved for based on the following equation [45]:

$$f = 1 - \frac{[([MMP]+[TIMP]+K_i^{app} - \sqrt{([MMP]+[TIMP]+K_i^{app})^2 - 4[MMP][TIMP]}}{2[MMP]} \quad (1)$$

f= fraction of activity, V_i/V_0

Specificity for MMP-X relative to MMP-Y was calculated according to the following formula:

$$\frac{WT\ K_i^{app}{}_{MMP-x} \Big/ Mut\ K_i^{app}{}_{MMP-x}}{WT\ K_i^{app}{}_{MMP-y} \Big/ Mut\ K_i^{app}{}_{MMP-y}} \quad (2)$$

Structural Modeling

Modeling of N-TIMP2 in complex with MMP-14_{CAT} and MMP-9_{CAT} was performed as in our previous study [38]. For modeling the mutations in the N-TIMP2 binding interface, the energy function optimized by Sharabi et al. [38, 46] was used. All mutations present in each N-TIMP2 mutant were simultaneously introduced into N-TIMP2 first with no backbone flexibility and then using backbone flexibility using the RosettaBackrub server [47]. The output of this protocol was a multiple-mutant structure along with its $\Delta\Delta G_{bind}$ value. The difference in molecular interactions due to introduction of each mutation was analyzed in the context of both structures, the N-TIMP2/MMP-14_{CAT} and the N-TIMP2/MMP-9_{CAT} structures to determine which type of interactions cause a specificity switch.

Results

N-TIMP2 library construction To obtain inhibitors that bind to either MMP-14_{CAT} or MMP-9_{CAT} with high affinity and high specificity, we constructed a small computationally designed combinatorial library that mutated only a few positions on the N-TIMP2 binding interface. We randomized eight positions in the direct N-TIMP2 binding interface (Figure 1A) to a limited set of amino acids, including either WT choice or mutation(s) observed to enhance binding affinity and/or specificity towards MMP-14_{CAT} in our previous study [38] (Table 1). Additional amino acid choices were included in the library when no degenerate codon could be found to simultaneously encode for only the desired choices. The designed library included 68480 different full-length N-TIMP2 sequences, and was enriched in sequences with enhanced specificity towards MMP-14_{CAT}. Sequencing of the library before selective sorting revealed that the clones in the library contained on average of 6±2 mutations per gene.

Selection of high specificity MMP-9 and MMP-14 binders. YSD technology was used to select specific binders for MMP-9_{CAT} and MMP-14_{CAT} in two parallel experiments. The N-TIMP2 library was expressed on the surface of yeast cells using the pCHA expression vector, where the yeast protein Aga2p

is fused to the C-terminus of N-TIMP2, leaving the N-terminus of the N-TIMP2 free for interaction with the target MMPs (Figure 2A). This arrangement is crucial since the N-terminus of N-TIMP2 mediates binding to the MMP active site and thereby facilitates proper inhibition of MMPs, as could be inferred from the crystal structure of N-TIMP2/MMP complexes and was confirmed in previous experiments [42, 48-50]. The c-Myc tag was used to monitor protein expression, through binding of an anti-c-Myc antibody and a fluorescently labelled secondary antibody against the anti-c-Myc. In our selection experiments, we used both positive and negative selection, by simultaneously incubating the N-TIMP2 libraries with two targets, MMP-14_{CAT} and MMP-9_{CAT}, labelled with two different fluorescent dyes, Dylight-488 and Dylight-650, respectively (Figure 2A). All sorts were performed using fluorescence activated cell sorting (FACS) (Figure 2B, C). To eliminate N-TIMP2 mutants that are not expressed (either due to deletions or due to frameshifts in the N-TIMP2 gene) we performed an initial pre-sorting round, by selecting the cells above a certain expression signal (Figure 2B).

Following this initial sorting, the libraries were incubated with 500 nM of MMP-14_{CAT} and 50 nM of MMP-9_{CAT} (Figure 2C). A lower concentration of MMP-9_{CAT} compared to MMP-14_{CAT} was necessary since N-TIMP2 has a higher natural affinity for MMP-9 as opposed to MMP-14 [38]. Under these conditions a distributed binding pattern was observed, where cells bound only MMP-14_{CAT}, only MMP-9_{CAT} or both MMP-14_{CAT} and MMP-9_{CAT} (Figure 2C). We further performed three rounds of sorting each time collecting 1% of all cells exhibiting the highest binding to MMP-14 (Supplementary Figure S1, upper panel) and separately to MMP-9 (Supplementary Figure S1, lower panel). From one round to the following, the concentration of the desired MMP was reduced while the concentration of the undesired MMP was raised, to make the binding specificity selection more stringent. After each round of sorting, ~20 colonies from both selections were randomly chosen for sequencing. Sequencing results showed an increasing convergence of certain mutations at particular N-TIMP2 positions with each round of selection. After the final round of selection, we obtained the specificity signatures for N-TIMP2 binding to MMP-14_{CAT} and to MMP-9_{CAT} (Figure 3A, B). The most outstanding result for the MMP-14_{CAT} selection is a unanimous consensus to asparagine at position 71 that replaces a WT valine (Figure 3A). The sequences of N-TIMP2 mutants in the MMP-9_{CAT} selection show a substantial consensus at position 4 for proline as opposed to the WT serine as well as a mutation from valine to isoleucine at position 71. At position 38, glutamine predominates the MMP-14_{CAT} selection, but a wild-type asparagine appears most frequently in the MMP-9_{CAT} selection. Positions 4, 38, and 71 hence, stand out as the most important specificity determining positions for MMP-14 and MMP-9 binding.

Understanding specificity signatures through modeling To understand the nature of enhanced specificity, we performed structural modeling of the engineered N-TIMP2 mutants when interacting with MMP-14 and MMP-9. At position 4, we see a strong preference for glutamate in the MMP-14_{CAT} selection while proline clearly predominates the MMP-9_{CAT} selection. Our modeling shows that a

glutamate at position 4 can form an intermolecular hydrogen bond with N231 on MMP-14_{CAT} but not with MMP-9_{CAT} (Figure 4A). A proline at position 4 fits better in the more hydrophobic environment of MMP-9_{CAT} but causes a steric clash with MMP-14_{CAT}, which could be removed only through substantial backbone conformational changes (Figure 4A). At position 38, glutamine predominates in the MMP-14_{CAT} selection, but a wild-type asparagine appears most frequently in the MMP-9_{CAT} selection. According to our modeling, Q38 makes a favorable hydrogen bond with N208 on MMP-14_{CAT}, but cannot make such a bond with the corresponding G197 on MMP-9_{CAT} (Figure 4B). It should be noted that glycine is conserved at this position in all the MMPs tested in this work except for MMP-14_{CAT} where this position is occupied by asparagine (Figure 1B). In the MMP-9_{CAT} selection, mutation to isoleucine predominates at position 71. This isoleucine packs against hydrophobic residues on MMP-9_{CAT}, namely F192 and Y179. Position 71 is highly enriched for a mutation to asparagine in the MMP-14_{CAT} selection; the asparagine could make a favorable hydrogen bond with Y203 on MMP-14_{CAT} (Figure 4C).

Purification and characterization of MMP-9_{CAT} and MMP-14_{CAT} inhibitors. To verify the success in binding specificity enhancement, six random N-TIMP2 mutants from each of the selection experiments were individually assessed for binding to MMP-14_{CAT} and MMP-9_{CAT} while displayed on the yeast surface (Figure 5A and C). The specificity of each mutant was evaluated by determining the ratio of the binding signal for the target MMP to that of the off-target MMP and then dividing by the same ratio for WT N-TIMP2. All tested mutants showed higher specificity towards the target MMP compared to that of WT N-TIMP2. In the MMP-14 selection experiment, we selected mutants 14D-4 and 14D-6 for further purification and characterization since they exhibited the highest specificity signal (Figure 5A). In the MMP-9 selection experiment, we chose mutants 9D-2 and 9D-6 since mutant 9D-2 exhibited the highest specificity signal (Figure 5C), whereas mutant 9D-6 recurred 3 out of 15 times among the sequenced clones. Table 2 lists the mutations present in the N-TIMP2 mutants chosen for purification and characterization from the designed library.

The four selected N-TIMP2 mutants and the WT N-TIMP2 were expressed and purified from *Pichia pastoris* yeast cells, which secrete the properly folded N-TIMP2 protein (Supplementary Figure S2)[50, 51]. The K_i^{app} of the inhibition of MMP-14_{CAT} and MMP-9_{CAT} by N-TIMP2 mutants was determined using an MMP enzyme activity assay in the absence and the presence of the N-TIMP2 inhibitor as previously described (Figure 5B and D) [38]. Table 3 summarizes the K_i^{app} values obtained for each N-TIMP2 mutant, for inhibition of MMP-14_{CAT} and MMP-9_{CAT}. All tested mutants showed a substantial increase in binding specificity towards the target MMP (Table 3 and 4). The best mutant from the MMP-14_{CAT} selection, 14D-6, with 8 mutations exhibited a specificity shift of ~60-fold. This specificity increase is due to ~3-fold improvement in affinity to the target MMP-14 and ~20-fold decrease in affinity to MMP-9 relative to WT N-TIMP2. The two expressed N-TIMP2 mutants from the MMP-9_{CAT} selection show similar double digit specificity enhancements values. The best mutant, 9D-6,

exhibits a 44-fold increase in binding specificity to MMP-9_{CAT} over MMP-$14_{CAT,}$ but a slightly worse affinity to MMP-9 compared to WT N-TIMP2. Thus, the specificity increase in this mutant comes through a great reduction in affinity to MMP-14_{CAT} relative to WT N-TIMP2. Note that the 9D-6 mutant exhibits nearly 1000-fold better binding affinity towards MMP-9_{CAT} vs. MMP-14_{CAT} (Table 3). Such high affinity differences, should be significant for preferential inhibition of MMP-9 but not MMP-14 in cellular environments.

To determine general binding specificity of our engineered MMP-14_{CAT} and MMP-9_{CAT} inhibitors, we measured their ability to inhibit a panel of additional MMP types, MMP-1_{CAT} (collagenase), MMP-2_{CAT} (gelatinase) and MMP-10_{CAT} (stromelysin). Table 4 shows that engineered N-TIMP2 mutants generally show reduced affinity to off-target MMPs that have not been used in our selection experiments. Higher specificity shifts are observed in the MMP-14_{CAT} selection, where mutant 14D-6 exhibits a 294-fold preference for MMP-14_{CAT} over MMP-10_{CAT}. The N-TIMP2 mutants from the MMP-9_{CAT} selection, especially 9D-6, are superior in absolute values of K_i^{app}, able to inhibit MMP-9_{CAT} at least 100 times better relative to all measured off-target MMPs (Table 3).

Discussion

Designing inhibitors that act against a single or narrow range of MMPs is clearly important for targeting MMPs in diseases and much effort in this direction has been recently reported [52]. In this work, we attempted to engineer such an inhibitor starting from the natural broad MMP inhibitor, N-TIMP2. Previously, we showed that the N-TIMP2/MMP binding interface is not optimized and contains many affinity- and specificity-enhancing mutations [38]. Specifically, positions 4, 35, 38 and 68 on TIMP were determined to be cold spots of binding [53], i.e. positions where several different mutations lead to increase in binding affinity towards MMP-14. We also determined that single mutations on N-TIMP2 in general, do not increase binding specificity by more than one order of magnitude. Here, we demonstrate that incorporation of 5-8 mutations into the N-TIMP2 sequence results in two orders of magnitude enhancement in binding specificity towards the target MMP. Among the combination of mutations found in this study, we frequently observe single mutations, previously identified as specificity-enhancing (e. g. at positions 4, 38, and 71). However, beneficial single mutations, when incorporated together, result in negative cooperativity, producing smaller specificity shifts for multiple mutants compared to the sum of shifts for single mutations.

As in many other engineering studies, the N-TIMP2 mutants reported here showed reduction of binding not only to the MMP used as a competitor but also to off-target MMPs not used in the selection procedure: MMP-1_{CAT}, MMP-2_{CAT}, and MMP-10_{CAT}. The amount of affinity reduction to off-target MMPs correlates well with the interface sequence identity between the target and the off-target MMP

(Figure 1B), exhibiting the lowest specificity shift against MMP-1_{CAT} in the MMP-14_{CAT} selection experiment and MMP-1_{CAT} and MMP-2_{CAT} in the MMP-9_{CAT} selection experiment. These results demonstrate that when similarity of off-targets is highest, the specificity for the target MMP is more difficult to achieve. Furthermore, the relatively small library of N-TIMP2 mutants, containing only ~70,000 mutants, could be used to evolve this protein to interact specifically with both MMP-14 and MMP-9. The same library is likely to produce specific binders for other MMPs, opening the way to future engineering studies.

The reported N-TIMP2 mutants exhibit specificity shifts similar to what has been observed in previous N-TIMP2 engineering studies. In our recent study, N-TIMP2 was engineered using a much larger library of 10^8 N-TIMP2 mutants and a more stringent selection procedure that included only the desired target, MMP-14_{CAT} [42]. In that work, 880-fold improvement in binding affinity for MMP-14_{CAT} was obtained, but small improvements in affinity were also reported for all but one of the off-target MMPs (MMP-1_{CAT}, MMP-2_{CAT}, and MMP-8_{CAT} but not MMP-10_{CAT}). In another study by Brew and colleagues, N-TIMP2 was engineered to bind with high specificity to MMP-1_{CAT}, and demonstrated 7-fold weaker affinity to MMP-1_{CAT}, no detectible binding to MMP-3_{CAT} and MMP-14_{CAT} and intermediate affinities to several other MMPs [22]. Together, these studies prove that N-TIMPs could be fine-tuned for better interaction with any MMP type, yet simultaneously discriminating against all off-target MMPs might be difficult due to relatively high sequence homology (65-80%) of various MMPs in the TIMP binding interface region. However, such discrimination might not be necessary for the development of anti-MMP drugs since the MMP inhibition pattern in real physiological environments depends on relative concentrations and localization of each MMP. Thus, each engineered N-TIMP2, with enhanced specificity and a certain set of binding affinities for each off-target MMP, might prove useful under particular MMP expression patterns.

We report for the first time, N-TIMP2 mutants engineered for MMP-9_{CAT} binding that exhibits 1000-fold better K_i^{app} for MMP-9_{CAT} vs. MMP-14_{CAT} and large discriminations against other tested MMPs. Such a mutant is likely to selectively inhibit MMP-9 under physiological conditions and thus could serve to probe the role of MMP-9 in various diseases. As several of our previously reported MMP-14-specific N-TIMP2 variants have already showed high potency in inhibiting cancer-related MMP activity in various cellular assays [42], the MMP-14- and MMP-9-specific mutants reported in this study present interesting candidates for further testing in cellular and *in vivo* studies. Overall, our results help to understand the molecular origins of binding specificity in TIMP/MMP interactions and facilitate development of cancer drugs and diagnostic tools targeting MMPs.

Acknowledgements We thank M. Lebendiker for help with protein purification and A. Zika for help with FACS experiments.

Funding This work was in part supported by the stage A grant from Yissum of the Hebrew University and Israel Science Foundation grant 1873/15 to J. M. S. N. P. is supported by the European Research Council "Ideas program" ERC-2013-StG (contract grant number: 336041). E.S.R. acknowledges support from U.S. National Institutes of Health grants R01CA154387 and R21CA205471.

Competing Financial Interests

The authors declare that they have no conflict of interest with respect to publication of this paper.

References

1. Rodriguez, D., Morrison, C. J. & Overall, C. M. (2010) Matrix metalloproteinases: what do they not do? New substrates and biological roles identified by murine models and proteomics, *Biochim Biophys Acta.* **1803**, 39-54.
2. Vandenbroucke, R. E. & Libert, C. (2014) Is there new hope for therapeutic matrix metalloproteinase inhibition?, *Nat Rev Drug Discov.* **13**, 904-927.
3. Coussens, L. M., Fingleton, B. & Matrisian, L. M. (2002) Matrix metalloproteinase inhibitors and cancer: trials and tribulations, *Science.* **295**, 2387-92.
4. Egeblad, M. & Werb, Z. (2002) New functions for the matrix metalloproteinases in cancer progression, *Nat Rev Cancer.* **2**, 161-74.
5. Rundhaug, J. E. (2005) Matrix metalloproteinases and angiogenesis, *J Cell Mol Med.* **9**, 267-85.
6. Deryugina, E. I. & Quigley, J. P. (2006) Matrix metalloproteinases and tumor metastasis, *Cancer metastasis reviews.* **25**, 9-34.
7. Overall, C. M. & Kleifeld, O. (2006) Tumour microenvironment - opinion: validating matrix metalloproteinases as drug targets and anti-targets for cancer therapy, *Nat Rev Cancer.* **6**, 227-39.
8. Lopez-Otin, C. & Matrisian, L. M. (2007) Emerging roles of proteases in tumour suppression, *Nat Rev Cancer.* **7**, 800-8.
9. Folgueras, A. R., Pendas, A. M., Sanchez, L. M. & Lopez-Otin, C. (2004) Matrix metalloproteinases in cancer: from new functions to improved inhibition strategies, *Int J Dev Biol.* **48**, 411-24.
10. Decock, J., Thirkettle, S., Wagstaff, L. & Edwards, D. R. (2011) Matrix metalloproteinases: protective roles in cancer, *J Cell Mol Med.* **15**, 1254-65.
11. Gilbreth, R. N. & Koide, S. (2012) Structural insights for engineering binding proteins based on non-antibody scaffolds, *Curr Opin Struct Biol.* **22**, 413-20.
12. Binz, H. K., Amstutz, P. & Pluckthun, A. (2005) Engineering novel binding proteins from nonimmunoglobulin domains, *Nat Biotechnol.* **23**, 1257-68.
13. Binz, H. K. & Pluckthun, A. (2005) Engineered proteins as specific binding reagents, *Curr Opin Biotechnol.* **16**, 459-69.
14. Gebauer, M. & Skerra, A. (2009) Engineered protein scaffolds as next-generation antibody therapeutics, *Curr Opin Chem Biol.* **13**, 245-55.
15. Sela-Passwell, N., Kikkeri, R., Dym, O., Rozenberg, H., Margalit, R., Arad-Yellin, R., Eisenstein, M., Brenner, O., Shoham, T., Danon, T., Shanzer, A. & Sagi, I. (2012) Antibodies targeting the catalytic zinc complex of activated matrix metalloproteinases show therapeutic potential, *Nat Med.* **18**, 143-7.
16. Devy, L., Huang, L., Naa, L., Yanamandra, N., Pieters, H., Frans, N., Chang, E., Tao, Q., Vanhove, M., Lejeune, A., van Gool, R., Sexton, D. J., Kuang, G., Rank, D., Hogan, S., Pazmany, C., Ma, Y. L., Schoonbroodt, S., Nixon, A. E., Ladner, R. C., Hoet, R., Henderikx, P., Tenhoor, C., Rabbani, S. A., Valentino, M. L., Wood, C. R. & Dransfield, D. T. (2009) Selective inhibition of matrix metalloproteinase-14 blocks tumor growth, invasion, and angiogenesis, *Cancer Res.* **69**, 1517-26.
17. Nam, D. H., Rodriguez, C., Remacle, A. G., Strongin, A. Y. & Ge, X. (2016) Active-site MMP-selective antibody inhibitors discovered from convex paratope synthetic libraries, *Proc Natl Acad Sci U S A.* **113**, 14970-14975.
18. Brew, K. & Nagase, H. (2010) The tissue inhibitors of metalloproteinases (TIMPs): an ancient family with structural and functional diversity, *Biochim Biophys Acta.* **1803**, 55-71.

19. Grossman, M., Tworowski, D., Dym, O., Lee, M. H., Levy, Y., Murphy, G. & Sagi, I. (2010) The intrinsic protein flexibility of endogenous protease inhibitor TIMP-1 controls its binding interface and affects its function, *Biochemistry.* **49**, 6184-92.
20. Wei, S., Chen, Y., Chung, L., Nagase, H. & Brew, K. (2003) Protein engineering of the tissue inhibitor of metalloproteinase 1 (TIMP-1) inhibitory domain. In search of selective matrix metalloproteinase inhibitors, *J Biol Chem.* **278**, 9831-4.
21. Wei, S., Kashiwagi, M., Kota, S., Xie, Z., Nagase, H. & Brew, K. (2005) Reactive site mutations in tissue inhibitor of metalloproteinase-3 disrupt inhibition of matrix metalloproteinases but not tumor necrosis factor-alpha-converting enzyme, *J Biol Chem.* **280**, 32877-82.
22. Bahudhanapati, H., Zhang, Y., Sidhu, S. S. & Brew, K. (2011) Phage display of tissue inhibitor of metalloproteinases-2 (TIMP-2): identification of selective inhibitors of collagenase-1 (metalloproteinase 1 (MMP-1)), *J Biol Chem.* **286**, 31761-70.
23. Huang, W., Suzuki, K., Nagase, H., Arumugam, S., Van Doren, S. R. & Brew, K. (1996) Folding and characterization of the amino-terminal domain of human tissue inhibitor of metalloproteinases-1 (TIMP-1) expressed at high yield in E. coli, *FEBS Lett.* **384**, 155-61.
24. Butler, G. S., Hutton, M., Wattam, B. A., Williamson, R. A., Knauper, V., Willenbrock, F. & Murphy, G. (1999) The specificity of TIMP-2 for matrix metalloproteinases can be modified by single amino acid mutations, *J Biol Chem.* **274**, 20391-6.
25. Dollery, C. M. & Libby, P. (2006) Atherosclerosis and proteinase activation, *Cardiovascular research.* **69**, 625-35.
26. Gomis-Ruth, F. X., Maskos, K., Betz, M., Bergner, A., Huber, R., Suzuki, K., Yoshida, N., Nagase, H., Brew, K., Bourenkov, G. P., Bartunik, H. & Bode, W. (1997) Mechanism of inhibition of the human matrix metalloproteinase stromelysin-1 by TIMP-1, *Nature.* **389**, 77-81.
27. Fernandez-Catalan, C., Bode, W., Huber, R., Turk, D., Calvete, J. J., Lichte, A., Tschesche, H. & Maskos, K. (1998) Crystal structure of the complex formed by the membrane type 1-matrix metalloproteinase with the tissue inhibitor of metalloproteinases-2, the soluble progelatinase A receptor, *Embo J.* **17**, 5238-48.
28. Maskos, K., Lang, R., Tschesche, H. & Bode, W. (2007) Flexibility and variability of TIMP binding: X-ray structure of the complex between collagenase-3/MMP-13 and TIMP-2, *J Mol Biol.* **366**, 1222-31.
29. Batra, J., Soares, A. S., Mehner, C. & Radisky, E. S. (2013) Matrix metalloproteinase-10/TIMP-2 structure and analyses define conserved core interactions and diverse exosite interactions in MMP/TIMP complexes, *PLoS One.* **8**, e75836.
30. Erijman, A., Aizner, Y. & Shifman, J. M. (2011) Multispecific recognition: mechanism, evolution, and design, *Biochemistry.* **50**, 602-11.
31. Fromer, M. & Shifman, J. M. (2009) Tradeoff between stability and multispecificity in the design of promiscuous proteins, *PLoS Comput Biol.* **5**, e1000627.
32. Humphris, E. L. & Kortemme, T. (2007) Design of multi-specificity in protein interfaces, *PLoS Comput Biol.* **3**, e164.
33. Shifman, J. M. & Mayo, S. L. (2003) Exploring the origins of binding specificity through the computational redesign of calmodulin, *Proc Natl Acad Sci U S A.* **100**, 13274-9.
34. Yosef, E., Politi, R., Choi, M. H. & Shifman, J. M. (2009) Computational design of calmodulin mutants with up to 900-fold increase in binding specificity, *J Mol Biol.* **385**, 1470-1480.
35. Sharabi, O., Erijman, A. & Shifman, J. M. (2013) Computational methods for controlling binding specificity, *Methods Enzymol.* **523**, 41-59.

36. Ernst, A., Avvakumov, G., Tong, J., Fan, Y., Zhao, Y., Alberts, P., Persaud, A., Walker, J. R., Neculai, A. M., Neculai, D., Vorobyov, A., Garg, P., Beatty, L., Chan, P. K., Juang, Y. C., Landry, M. C., Yeh, C., Zeqiraj, E., Karamboulas, K., Allali-Hassani, A., Vedadi, M., Tyers, M., Moffat, J., Sicheri, F., Pelletier, L., Durocher, D., Raught, B., Rotin, D., Yang, J., Moran, M. F., Dhe-Paganon, S. & Sidhu, S. S. (2013) A strategy for modulation of enzymes in the ubiquitin system, *Science*. **339**, 590-5.
37. Cohen, I., Kayode, O., Hockla, A., Sankaran, B., Radisky, D. C., Radisky, E. S. & Papo, N. (2016) Combinatorial protein engineering of proteolytically resistant mesotrypsin inhibitors as candidates for cancer therapy, *The Biochemical journal*. **473**, 1329-41.
38. Sharabi, O., Shirian, J., Grossman, M., Lebendiker, M., Sagi, I. & Shifman, J. (2014) Affinity- and Specificity-Enhancing Mutations Are Frequent in Multispecific Interactions between TIMP2 and MMPs, *PLoS ONE*. **9**, e93712.
39. Sharabi, O., Shirian, J. & Shifman, J. M. (2013) Predicting affinity- and specificity-enhancing mutations at protein-protein interfaces, *Biochem Soc Trans.* **41**, 1166-9.
40. Pepper, L. R., Cho, Y. K., Boder, E. T. & Shusta, E. V. (2008) A decade of yeast surface display technology: where are we now?, *Combinatorial chemistry & high throughput screening.* **11**, 127-34.
41. Mata-Fink, J., Kriegsman, B., Yu, H. X., Zhu, H., Hanson, M. C., Irvine, D. J. & Wittrup, K. D. (2013) Rapid conformational epitope mapping of anti-gp120 antibodies with a designed mutant panel displayed on yeast, *J Mol Biol.* **425**, 444-56.
42. Arkadash, V., Yosef, G., Shirian, J., Cohen, I., Horev, Y., Grossman, M., Sagi, I., Radisky, E. S., Shifman, J. M. & Papo, N. (2017) Development of high-affinity and high-specificity inhibitors of metalloproteinase 14 through computational design and directed evolution, *J Biol Chem.* **292**, 3481-3495.
43. Erijman, A., Dantes, A., Bernheim, R., Shifman, J. M. & Peleg, Y. (2011) Transfer-PCR (TPCR): a highway for DNA cloning and protein engineering, *J Struct Biol.* **175**, 171-7.
44. Batra, J., Robinson, J., Soares, A. S., Fields, A. P., Radisky, D. C. & Radisky, E. S. (2012) Matrix metalloproteinase-10 (MMP-10) interaction with tissue inhibitors of metalloproteinases TIMP-1 and TIMP-2: binding studies and crystal structure, *J Biol Chem.* **287**, 15935-46.
45. Murphy, D. J. (2004) Determination of accurate KI values for tight-binding enzyme inhibitors: an in silico study of experimental error and assay design, *Analytical biochemistry.* **327**, 61-7.
46. Sharabi, O., Dekel, A. & Shifman, J. M. (2011) Triathlon for energy functions: Who is the winner for design of protein–protein interactions?, *Proteins: Structure, Function, and Bioinformatics.* **79**, 1487-1498.
47. Lauck, F., Smith, C. A., Friedland, G. F., Humphris, E. L. & Kortemme, T. (2010) RosettaBackrub--a web server for flexible backbone protein structure modeling and design, *Nucleic Acids Res.* **38**, W569-75.
48. Arumugam, S., Gao, G., Patton, B. L., Semenchenko, V., Brew, K. & Van Doren, S. R. (2003) Increased backbone mobility in beta-barrel enhances entropy gain driving binding of N-TIMP-1 to MMP-3, *J Mol Biol.* **327**, 719-34.
49. Wingfield, P. T., Sax, J. K., Stahl, S. J., Kaufman, J., Palmer, I., Chung, V., Corcoran, M. L., Kleiner, D. E. & Stetler-Stevenson, W. G. (1999) Biophysical and functional characterization of full-length, recombinant human tissue inhibitor of metalloproteinases-2 (TIMP-2) produced in Escherichia coli. Comparison of wild type and amino-terminal alanine appended variant with implications for the mechanism of TIMP functions, *J Biol Chem.* **274**, 21362-8.
50. Fernandez, C. A., Butterfield, C., Jackson, G. & Moses, M. A. (2003) Structural and functional uncoupling of the enzymatic and angiogenic inhibitory activities of tissue inhibitor of

metalloproteinase-2 (TIMP-2): loop 6 is a novel angiogenesis inhibitor, *J Biol Chem.* **278**, 40989-95.
51. Masuda, T., Tamaki, S., Kaneko, R., Wada, R., Fujita, Y., Mehta, A. & Kitabatake, N. (2004) Cloning, expression and characterization of recombinant sweet-protein thaumatin II using the methylotrophic yeast Pichia pastoris, *Biotechnology and bioengineering.* **85**, 761-9.
52. Radisky, E. S., Raeeszadeh-Sarmazdeh, M. & Radisky, D. C. (2017) Therapeutic Potential of Matrix Metalloproteinase Inhibition in Breast Cancer, *J Cell Biochem.* **118**, 3531-3548.
53. Shirian, J., Sharabi, O. & Shifman, J. M. (2016) Cold-spots in Protein Binding, *in preparation*.
54. Elkins, P. A., Ho, Y. S., Smith, W. W., Janson, C. A., D'Alessio, K. J., McQueney, M. S., Cummings, M. D. & Romanic, A. M. (2002) Structure of the C-terminally truncated human ProMMP9, a gelatin-binding matrix metalloproteinase, *Acta crystallographica Section D, Biological crystallography.* **58**, 1182-92.
55. Chao, G., Lau, W. L., Hackel, B. J., Sazinsky, S. L., Lippow, S. M. & Wittrup, K. D. (2006) Isolating and engineering human antibodies using yeast surface display, *Nat Protoc.* **1**, 755-68.

Figures Legends

Figure 1: (A) Structural alignment of MMP-9_{CAT} shown in magenta (PDB: 1L6J) and MMP-14_{CAT} shown in green (PDB: 1BUV) in complex with N-TIMP2 shown in blue. Red spheres indicate positions where mutations were allowed in the designed combinatorial N-TIMP2 library and are labelled with their WT identity. Yellow sphere represents Zn^{2+} atom in the MMP active site.
(B) **Left panel** A pairwise alignment of residues on MMP-1_{CAT}, MMP-2_{CAT}, MMP-9_{CAT}, MMP-10_{CAT}, and MMP-14_{CAT} (generated with the aid of EMBL Clustal Omega). Residues located in the WT N-TIMP2:MMP interface are colour coded according to chemical character of their side chains. Red represents hydrophobic residues, green represents hydrophilic residues, pink represents positively charged residues and blue represents negatively charged residues. These interface residues are at a distance of 4Å or less from N-TIMP2. Asterisks indicate that there is a consensus at a particular position. **Right panel** Percent of amino-acid identity between binding interface residues for various pairs of MMPs is shown.

Figure 2: (A) Schematic representation of N-TIMP2 displayed on the yeast surface (adapted from Chao et al.[56]). The N-terminus of N-TIMP2 is free and facing away from the yeast surface. (B) Expression of the construct was monitored by FACS by fluorescently labelled antibodies (red burst in panel A) that bind the c-Myc tag in the construct. (C) Binding of N-TIMP2 to catalytic domains of MMP proteins in solution was monitored by FACS by incubating the N-TIMP2 library with two MMP targets (MMP-9_{CAT}) and (MMP-14_{CAT}) simultaneously and using two different fluorescent labels for each MMP proteins (yellow and blue bursts in panel A). Red polygons represent sample cell collection gates, A for MMP-14_{CAT} and B for MMP-9_{CAT}. The figure here was produced in the initial sorting round on the focused library.

Figure 3: Logos based on sequencing of evolved N-TIMP2 libraries after 3 rounds of binding selection for MMP-14_{CAT} (A) and MMP-9_{CAT} (B). The logos were made through http://weblogo.berkeley.edu/logo.cgi. The WT identity of each position is shown below each logo and the size of the amino acid corresponds to its frequency among the selected sequences. The total height of the stack represents conservation at that position. Green, purple, blue, red and black letters respectively represent polar, neutral, basic, acidic and hydrophobic amino acids. Only eight binding interface positions on N-TIMP2 are shown. Additional unintended mutations were observed in more than 50% of the sequences, at an average frequency of one and a half mutations per sequence.

Figure 4: Interactions observed in computationally modeled structures of specificity enhancing mutations of N-TIMP2. N-TIMP2 is depicted in cyan and MMP-9_{CAT} or MMP-14_{CAT} is depicted in green; polar contacts are shown as red dotted lines. MMP residues shown in sticks are not further than 4Å away from the highlighted N-TIMP2 residue. Hydrogen atoms are shown as necessary for depiction of hydrogen bonds. (A) The glutamate at position 4 interacting with MMP-9_{CAT} (leftmost panel) and MMP-14_{CAT} (middle panel). Rightmost panel depicts backbone movement necessary in MMP-14_{CAT} to accommodate for proline occupying position 4 on N-TIMP2 as seen from structural alignment before and after modeling with backbone flexibility. The MMP-14_{CAT} structure before introduction of backbone flexibility is shown in red and after is shown in green, N-TIMP2 is shown in cyan. Arrows indicate region within which backbone was altered. (B) Interactions of Gln at position 38 with both MMPs are shown (C) Interactions of Ile and Asn at position 71 in the context of both MMPs are shown.

Figure 5: (A, C) Binding specificity of selected N-TIMP2 mutant yeast colonies assessed by FACS. Binding is determined by the average signal of fluorescence of yeast cells caused by fluorescently labelled MMP. Binding specificity is determined in the following manner in the case of MMP-14_{CAT}: $(\text{MMP-14}_{mut}/\text{MMP-14}_{wt})/(\text{MMP-9}_{mut}/\text{MMP-9}_{wt})$, and vice-versa for MMP-9_{CAT}.
(B, D) Enzyme activity assays with inhibition by WT N-TIMP2 or mutants expressed in *P. pastoris*. Data points represent an average of at least three experiments. Curves were fit to *equation 1*. (B) Enzyme

activity experiments performed with MMP-14_{CAT}. (D) Enzyme activity experiments performed with MMP-9_{CAT}.

Table 1: Design of the small focused N-TIMP-2 library Desired amino acid choices display mutations that were tested experimentally and showed enhanced binding specificity of N-TIMP-2 towards MMP-14_{CAT} in our previous work when introduced as single mutations. The rightmost column shows all the amino acid choices encoded in the library at each position, including extra choices that appeared due to encoding each position with a particular degenerate codon. WT amino acid identities are underlined.

N-TIMP-2 Position	Desired Amino Acid Choices	Degenerate Codon	Actual Encoded Amino Acids
4	A, Q, E, S	BMR	A, Q, E, P, S, stop
6	R, V	SKN	R, G, L, V
35	E, I, K	RWA	E, I, K, V
38	N, Q	MAN	N, Q, H, K
68	S, W, Y	WRS	R, N, C, K, S, W, Y, stop
71	N, V	RWY	N, D, I, V
97	R, H	CRY	R, H
99	T, Y	WMY	N, S, T, Y

Table 2: Sequences of the N-TIMP2 mutants chosen for expression and purification Mutations in N-TIMP2 variants chosen to be assayed *in vitro* as purified proteins from the small designed combinatorial focused N-TIMP2 library. "--" indicates that the WT identity at this particular position was maintained. Mutant 14D-6 contains a mutation, V18M, which was not in initial design of the library.

Position:	4	6	35	38	68	71	97	99	Additional mutations
WT	**S**	**V**	**I**	**N**	**S**	**V**	**H**	**T**	
14D-4	**E**	**--**	**--**	**Q**	**--**	**N**	**R**	**S**	
14D-6	**E**	**R**	**V**	**Q**	**N**	**N**	**R**	**--**	**V18M**
9D-2	**P**	**--**	**V**	**--**	**N**	**I**	**R**	**--**	
9D-6	**P**	**G**	**V**	**--**	**N**	**I**	**--**	**N**	

Table 3: Inhibitory activities of the purified proteins. Purified N-TIMP2 mutants were assayed for their ability to inhibit MMP-14_{CAT} and MMP-9_{CAT}. K_i^{app} values were obtained from at least three such

assay experiments for each protein and averaged, each value is reported as K_i^{app} ± S.D. The exceptions are a few experiments where very high mutant concentration was required and thus only one experiment was performed. The boldface values of each cell shows the relative inhibitory affinity for the target vs. off-target MMP: K_i^{app} for MMP-target/K_i^{app} for MMP-x, where target is MMP-14_{CAT} or MMP-9_{CAT} and x is any off-target MMP.

	K_i^{app} of binding (nM)				
	MMP-14_{CAT}	**MMP-9_{CAT}**	**MMP-1_{CAT}**	**MMP-2_{CAT}**	**MMP-10_{CAT}**
WT	2.52±0.32	0.12±0.02	0.25±0.02	2.65±0.76	4.3±0.29
14D-4	1.02±0.62	1.28±0.18	0.31±0.03	83.96±4.57	78.91±41.55
	1.0	**0.80**	**3.38**	**0.01**	**0.01**
14D-6	0.89±0.06	2.43±0.90	0.78±0.21	224.5	446.35±167.09
	1.0	**0.37**	**1.14**	**0.004**	**0.002**
9D-2	105.73±4.78	0.15±0.04	0.11±0.02	3.53±0.34	>300
	0.001	**1.0**	**1.36**	**0.04**	**<0.0005**
9D-6	463.50±33.16	0.50±0.12	9.53±3.21	38.89±2.50	>300
	0.001	**1.0**	**0.05**	**0.01**	**<0.002**

Table 4: Specificity shifts of N-TIMP2 mutants in favor of MMP-14_{CAT} or MMP-9_{CAT} as compared to off-target MMPs Specificity shifts were calculated according to eq. 2. The specificity shifts were calculated relative to MMP-14_{CAT} for the mutants engineered to bind to MMP-14_{CAT} and were calculated relative to MMP-9_{CAT} for the MMP-9_{CAT} engineered mutants.

	Specificity shifts for MMP binding				
N-TIMP2 mutant	MMP-14_{CAT}	MMP-9_{CAT}	MMP-1_{CAT}	MMP-2_{CAT}	MMP-10_{CAT}
14D-4	-	26	3	78	45
14D-6	-	57	9	240	294
9D-2	34	-	0.35	1	>56
9D-6	44	-	9	4	>17

Figure 1

(a)

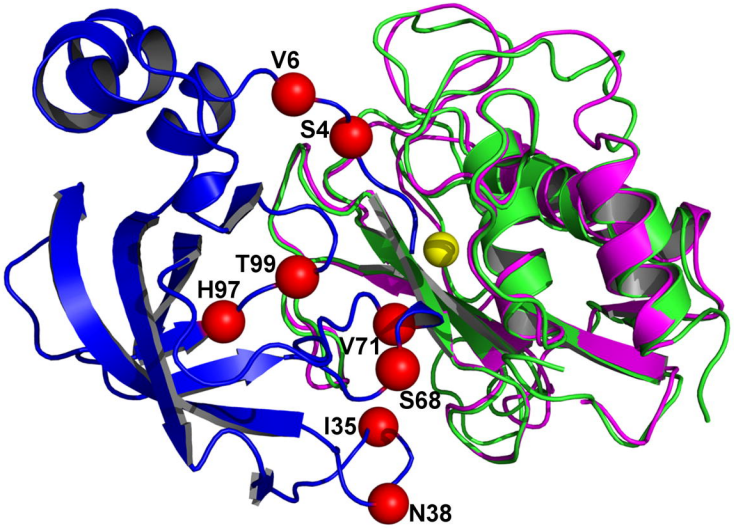

(b)

```
MMP-1   160 M I S F V R G D H R D N S P F D G P G G N L A H Q P G P G 190
MMP-2   170 M I N F G R W E H G D G Y P F D G K D G L L A H A P G T G 200
MMP-9   167 V I Q F G V A E H G D G Y P F D G K D G L L A H P P G P G 197
MMP-10  159 M I S F A V K E H G D F Y S F D G P G H S L A H P P G P G 189
MMP-14  178 M I F F A E G F H G D S T P F D G E G G F L A H F P G P N 208
                * *   * *   * * *       * * *   * *

MMP-1   191 I G G D V A A H E L G H S L G L S H S T D I G A Y P S Y 240
MMP-2   201 V G G D V A A H E F G H A M G L E H S Q D P G A A P I Y 223
MMP-9   198 I Q G D V A A H E F G H A L G L D H S S V P E A Y P M Y 423
MMP-10  190 L Y G D V A A H E L G H S L G L F H S A N T E A Y P L Y 239
MMP-14  209 I G G D V A V H E L G H A L G L E H S S D P S A A P F Y 261
            * * * * * * * * * * * * * * * * * * * * * * * * *
```

Interface Identity		
	MMP-9	MMP-14
MMP-1	71.9%	71.9%
MMP-2	87.5%	65.6%
MMP-9	-	65.6%
MMP-10	68.8%	68.8%
MMP-14	65.6%	-

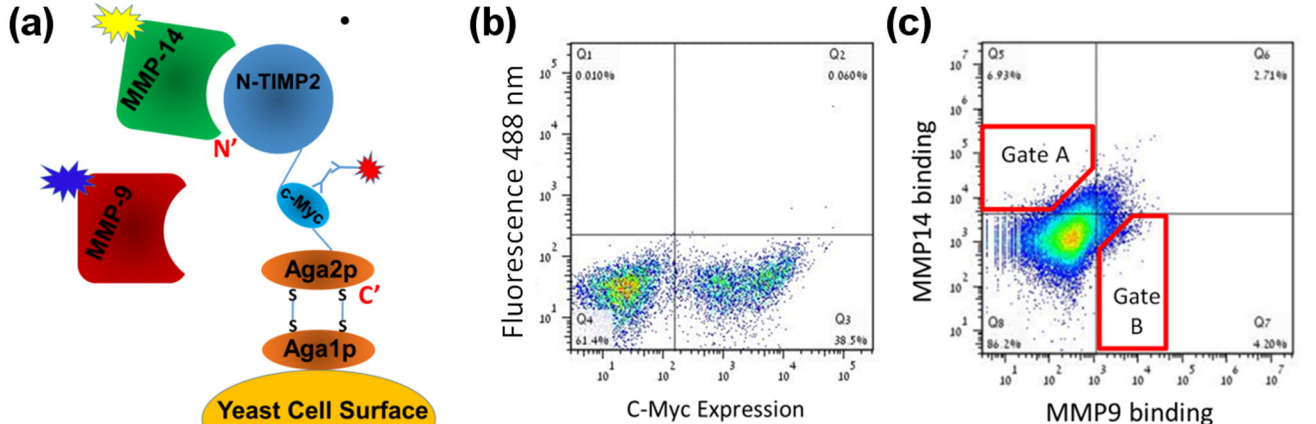
(a)
MMP-14
N-TIMP2
N'
MMP-9
c-Myc
Aga2p
C'
Aga1p
Yeast Cell Surface
(b)
Fluorescence 488 nm
C-Myc Expression
Q1
0.010%
Q2
0.060%
Q4
61.4%
Q3
38.5%
(c)
MMP14 binding
MMP9 binding
Gate A
Gate B
Q5
6.93%
Q6
2.71%
Q8
86.2%
Q7
4.20%

Figure 2

Figure 3

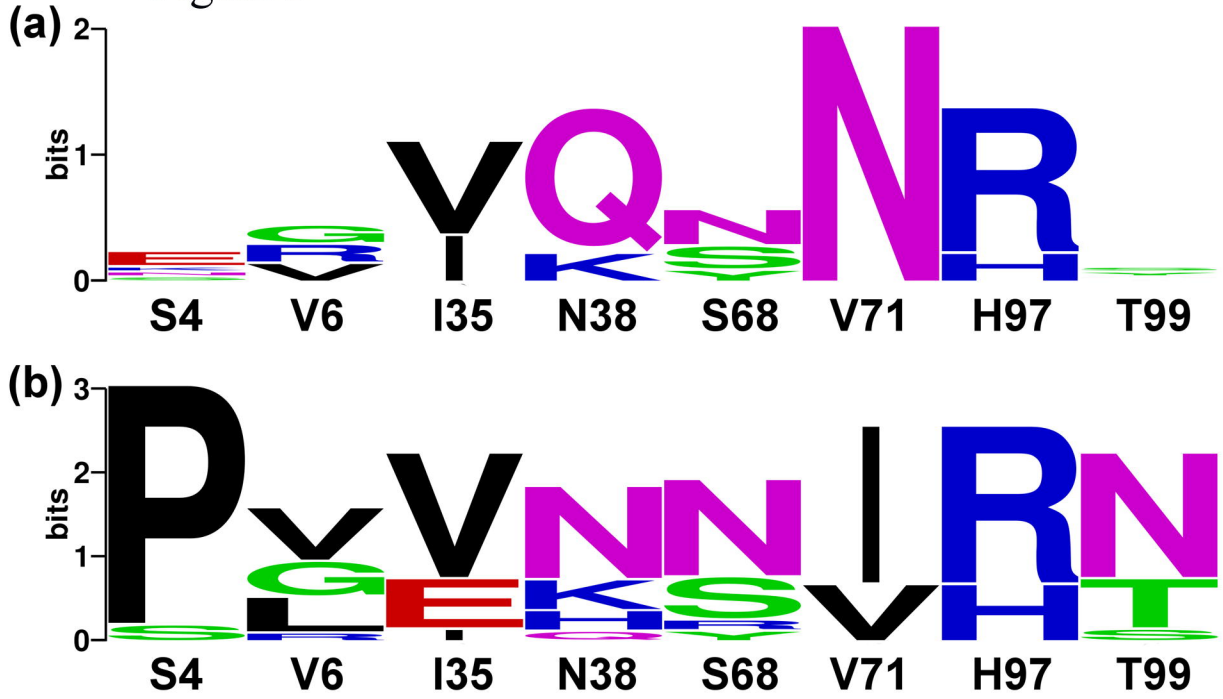
(a)
bits
2
1
0
S4
V6
I35
N38
S68
V71
H97
T99
(b)
bits
3
2
1
0
S4
V6
I35
N38
S68
V71
H97
T99

Figure 4

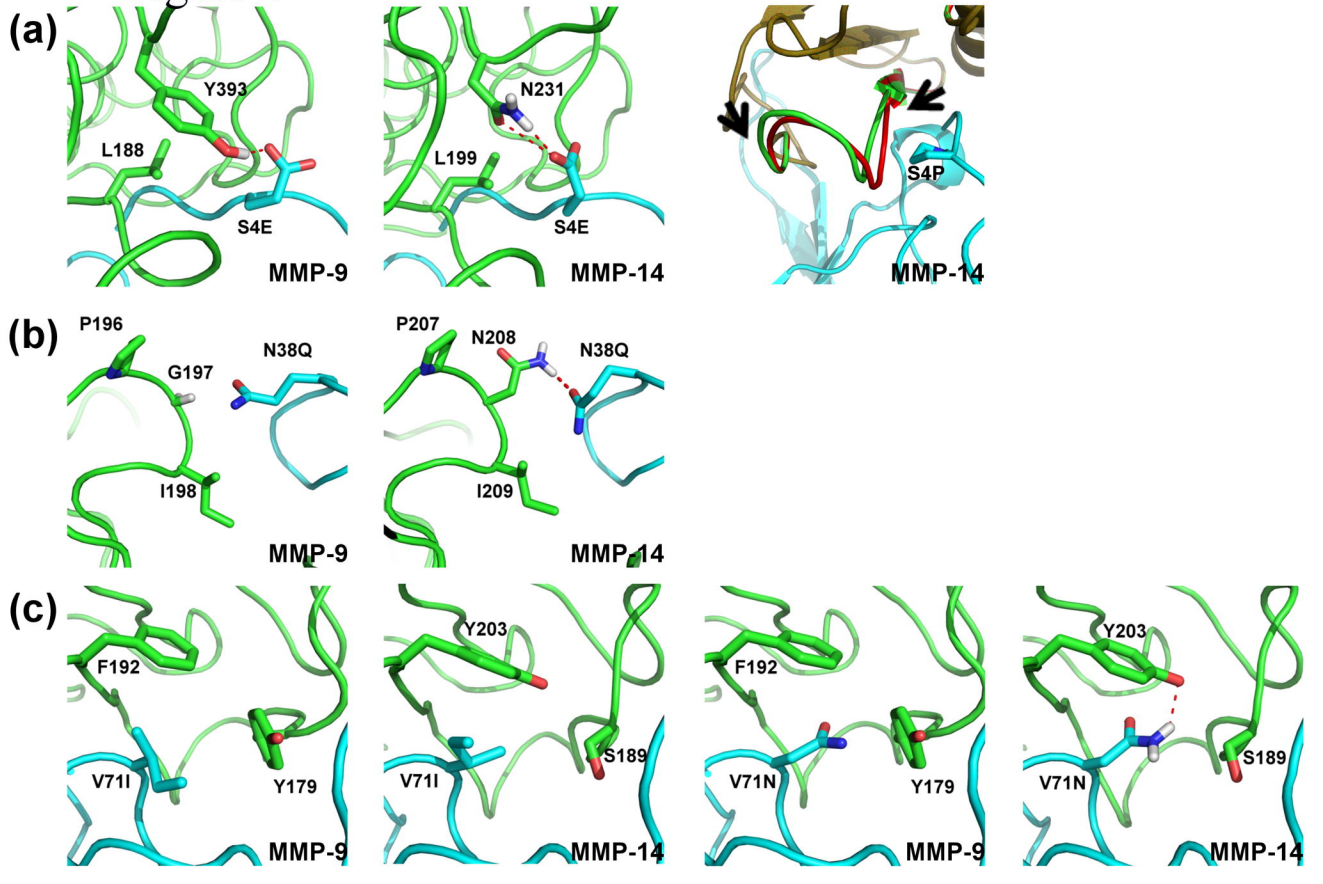
(a)
Y393
L188
S4E
MMP-9
N231
L199
S4E
MMP-14
S4P
MMP-14
(b)
P196
G197
N38Q
I198
MMP-9
P207
N208
N38Q
I209
MMP-14
(c)
F192
V71I
Y179
MMP-9
Y203
V71I
S189
MMP-14
F192
V71N
Y179
MMP-9
Y203
V71N
S189
MMP-14

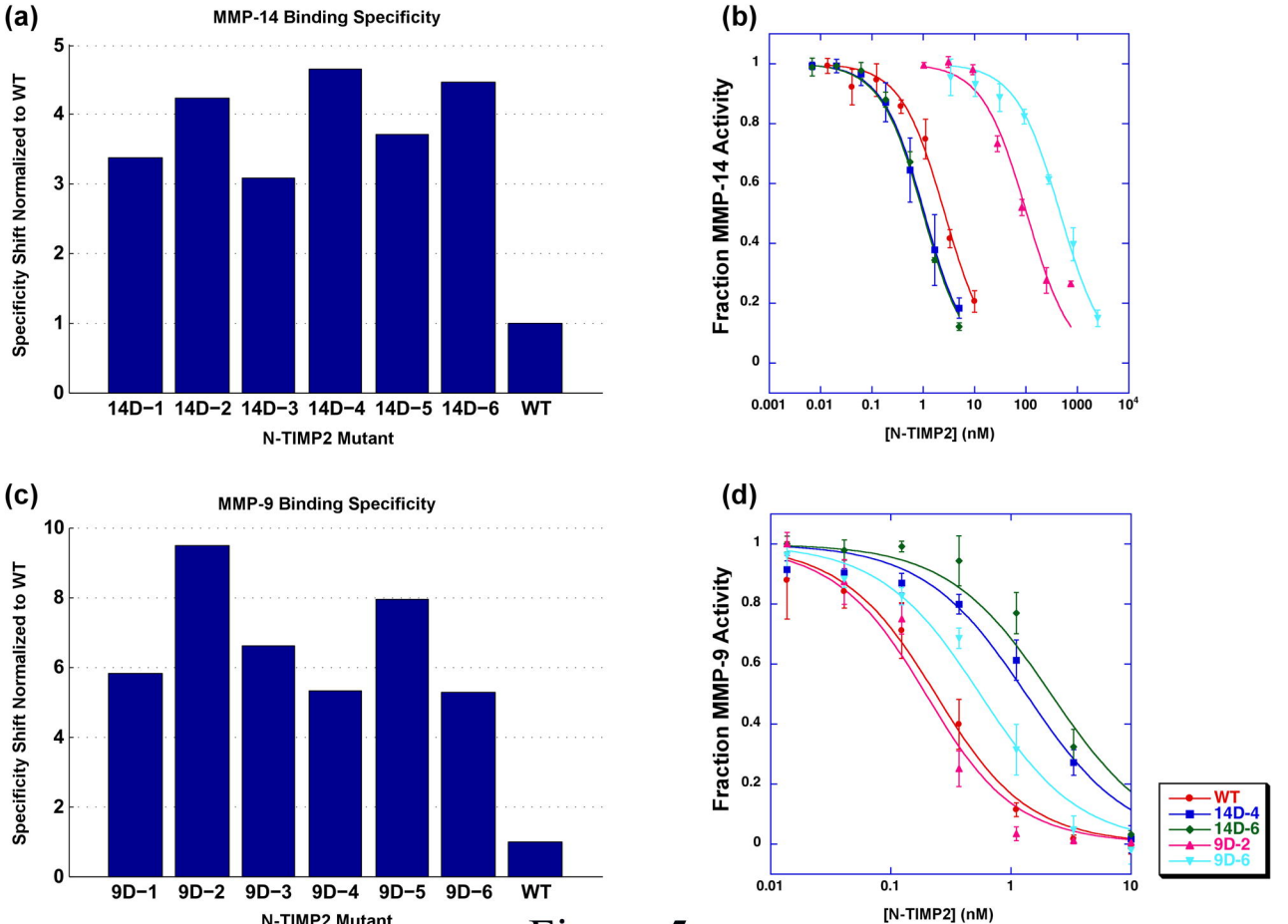
(a)
MMP-14 Binding Specificity
Specificity Shift Normalized to WT
0
1
2
3
4
5
14D−1
14D−2
14D−3
14D−4
14D−5
14D−6
WT
N-TIMP2 Mutant
(b)
Fraction MMP-14 Activity
0
0.2
0.4
0.6
0.8
1
0.001
0.01
0.1
1
10
100
1000
10^4
[N-TIMP2] (nM)
(c)
MMP-9 Binding Specificity
Specificity Shift Normalized to WT
0
2
4
6
8
10
9D−1
9D−2
9D−3
9D−4
9D−5
9D−6
WT
N-TIMP2 Mutant
(d)
Fraction MMP-9 Activity
0
0.2
0.4
0.6
0.8
1
0.01
0.1
1
10
[N-TIMP2] (nM)
WT
14D-4
14D-6
9D-2
9D-6

Figure 5